ARTICLES

Journal of Semiconductors
(2022) 43, 112801
doi: 10.1088/1674-4926/43/11/112801

Clarifying the atomic origin of electron killers in β-Ga_2O_3 from the first-principles study of electron capture rates

Zhaojun Suo[1, 2], Linwang Wang[1, †], Shushen Li[1, 2], and Junwei Luo[1, 2, †]

[1]State Key Laboratory of Superlattices and Microstructures, Institute of Semiconductors, Chinese Academy of Sciences, Beijing 100083, China
[2]Center of Materials Science and Optoelectronics Engineering, University of Chinese Academy of Sciences, Beijing 100049, China

Abstract: The emerging wide bandgap semiconductor β-Ga_2O_3 has attracted great interest due to its promising applications for high-power electronic devices and solar-blind ultraviolet photodetectors. Deep-level defects in β-Ga_2O_3 have been intensively studied towards improving device performance. Deep-level signatures E_1, E_2, and E_3 with energy positions of 0.55–0.63, 0.74–0.81, and 1.01–1.10 eV below the conduction band minimum have frequently been observed and extensively investigated, but their atomic origins are still under debate. In this work, we attempt to clarify these deep-level signatures from the comparison of theoretically predicted electron capture cross-sections of suggested candidates, Ti and Fe substituting Ga on a tetrahedral site (Ti_{GaI} and Fe_{GaI}) and an octahedral site (Ti_{GaII} and Fe_{GaII}), to experimentally measured results. The first-principles approach predicted electron capture cross-sections of Ti_{GaI} and Ti_{GaII} defects are 8.56×10^{-14} and 2.97×10^{-13} cm^2, in good agreement with the experimental values of E_1 and E_3 centers, respectively. We, therefore, confirmed that E_1 and E_3 centers are indeed associated with Ti_{GaI} and Ti_{GaII} defects, respectively. Whereas the predicted electron capture cross-sections of Fe_{Ga} defect are two orders of magnitude larger than the experimental value of the E_2, indicating E_2 may have other origins like C_{Ga} and Ga_i, rather than common believed Fe_{Ga}.

Key words: wide bandgap semiconductor; defects; carrier trap; electron-phonon coupling; first-principles calculation

Citation: Z J Suo, L W Wang, S S Li, and J W Luo, Clarifying the atomic origin of electron killers in β-Ga_2O_3 from the first-principles study of electron capture rates[J]. *J. Semicond.*, 2022, 43(11), 112801. https://doi.org/10.1088/1674-4926/43/11/112801

1. Introduction

Monoclinic gallium sesquioxide (β-Ga_2O_3) has drawn a lot of attention due to its ultra-wide bandgap (~4.9 eV) and ultra-high breakdown electrical fields, which make it promising in the application of power electronics and deep-ultraviolet optoelectronics[1, 2]. In particular, it owns a high Baliga's figure of merit more than four times that of GaN and SiC[1], making it to be an excellent candidate for power semiconductor devices operating in high-frequency circuits[1, 2]. Besides, the β-Ga_2O_3 devices have the advantages of high radiation hardness, high-temperature stability, potentially low cost due to the earth-abundant material, and ease to manufacture massively due to its compatibility with Si microelectronic technology. In the application of semiconductors, defects can significantly influence the performance of devices. For example, they may bring in deep levels inside the bandgap to trap the carriers or even become the nonradiative recombination centers to kill the free carriers, deteriorating the performance of devices[3].

In β-Ga_2O_3, three signature levels (E_1, E_2, and E_3) have been frequently observed in the deep-level transient spectroscopy (DLTS) measurements irrespective of different types of measured β-Ga_2O_3 samples, including bulk crystals grown by the Czochralski method (CZ)[4] and edge-defined film-fed growth (EFG)[5], and epitaxial thin films fabricated by metalorganic chemical vapor deposition (MOCVD)[6] and hydride vapor phase epitaxy (HVPE)[7]. Specifically, E_1 is 0.55–0.63 eV, E_2 is 0.74–0.81 eV, and E_3 is 1.01–1.10 eV below the conduction band minimum (CBM) of β-Ga_2O_3[4–7]. The DLTS measurements also obtained the electron capture cross-sections, which are 10^{-14}–10^{-13}, 10^{-16}–10^{-15}, and 10^{-14}–10^{-13} cm^2[4, 5, 7], respectively, for these three signature levels. Table 1 summarizes these experimentally measured defect signature levels and corresponding electron capture cross-sections. These signature levels have been assigned to different types of defects, such as intrinsic defects or extrinsic impurities[8]. For instance, (i) the origin of the E_1 and E_3 centers used to be regarded as the transition metal impurities presenting at the Ga lattice sites[9], including Fe_{Ga} and Co_{Ga}[4]. (ii) The E_2 center was initially suggested to be the Fe_{Ga} defects by Ingebrigtsen *et al.*[8]. Zimmerman *et al.*[10] further distinguished that there are two overlapping DTLS peaks, labeled as E_{2a} (0.66 eV) and E_{2b} (0.73 eV) instead of a single E_2. These two signatures have then been assigned to the Fe substituting Ga on a tetrahedral site (Fe_{GaI}) and an octahedral site (Fe_{GaII}), respectively, based on the energy levels and the concentration ratio[10]. Recently, Zimmermann *et al.*[11] provided additional evidence to support the above conclusion regarding the good agreement of absorption cross-section between first-principles calculations of the Fe_{Ga} defect and the experimental results from steady-state photo-capacitance spectra measurements. (iii) The E_3 trapping center has been suggested as oxygen vacancy (V_O)[12], or substitutional transition-metal defects (e.g., Fe_{Ga} or Ti_{Ga})[9]. However, the calculated V_O defect

Correspondence to: L W Wang, lwwang@semi.ac.cn; J W Luo, jwluo@semi.ac.cn
Received 27 APRIL 2022; Revised 29 MAY 2022.

Table 1. Compilation of energy levels (below the CBM and unit in eV) and electron capture cross-sections of three significant defect traps in β-Ga_2O_3 obtained from different DLTS measurements.

Signature	E_1	E_2	E_3	Reference
Level (eV)	0.55	0.74	1.04	Ref. [4]
	0.63	0.81	1.03	Ref. [5]
	–	0.80	1.10	Ref. [6]
σ_n (cm^2)	$(0.3–3)\times10^{-14}$	$(0.3–3)\times10^{-15}$	$(0.6–6)\times10^{-13}$	Ref. [4]
	$(0.3–5)\times10^{-13}$	$(0.2–1.2)\times10^{-15}$	2×10^{-14}–1×10^{-12}	Ref. [7]
	2.7×10^{-13}	6×10^{-15}	1×10^{-13}	Ref. [5]

level is located at 1.67–2.46 eV (below the CBM)[13], which is much deeper than E_3 at 1.01–1.10 eV and thus can be ruled out. Zimmerman *et al.*[10] then assigned the E_3 center as a defect of Ti substituting Ga on an octahedral site (denoted as Ti_{GaII}) based on a strong correlation in concentration between the E_3 defect and the Ti ions present in the samples and a good agreement in energy position between the E_3 level and the Ti_{GaII} defect, which is obtained by the hybrid functional calculations. So far, Fe- and Ti-related defects are considered as the most possible candidates for E_1, E_2, and E_3 centers not only due to the above arguments but also because they can be introduced to β-Ga_2O_3 unintentionally in fabrications. For example, Fe is the most common contaminant in manufacturing. Ti is often used as Ohmic contact for β-Ga_2O_3 devices[1, 14]. However, most identifications are made based purely on matching the energy levels, which could be accidental.

Generally, the DLTS is a highly sensitive analytical technique that is used to measure the energy positions of defects and obtain the carrier capture cross-sections, but without the capability to obtain information about the configuration and elements of the defects[4]. The first-principles calculations are therefore used to explore the atomic origin of these defect levels by examining their defect levels. One challenge in previous theoretical studies of the defect levels is that only the predicted transition energies can be compared with experimental data. Therefore, the identification of the atomic origin for a special defect level is still a difficult task. Fortunately, the newly developed first-principles approach for carrier capture cross-sections enables us to examine the defect candidates utilizing a combination of both the energy level and carrier capture cross-section for each center. In this work, we use this approach to verify the well-established defect candidates of Ti_{Ga} and Fe_{Ga} for the three signatures in β-Ga_2O_3 by performing the first-principles calculations for both defect transition level and electronic capture cross-section. The calculated transition levels of Ti_{GaI} and Ti_{GaII} from a charge state $q = +1$ to a charge state $q = 0$ are 0.59 and 1.08 eV below the CBM within the ranges of DLTS measured E_1 (0.55–0.63 eV) and E_3 (1.01–1.10 eV), respectively. This excellent agreement is consistent with previous first-principles calculations[10]. In particular, the calculated electron capture cross-sections of Ti_{GaI} and Ti_{GaII} defects are both around 10^{-14}–10^{-13} cm^2 and thus are also in excellent agreement with experimental results of E_1 and E_3 centers[4, 5, 7, 10, 15]. Subsequently, we can safely conclude that the Ti_{GaI} and Ti_{GaII} defects are responsible for DTLS observed E_1 and E_3 centers, respectively. However, the calculated electron capture cross-section of Fe_{Ga} defects is around 10^{-13} cm^2, which is about two orders of magnitude larger than that of DLTS measured E_2 center. Such large disagreement indicates that E_2 has other origins than Fe_{Ga}, although the defect levels of Fe_{Ga} are in good agreement with the E_2 (or E_{2a}, and E_{2b}) center.

Table 2. Lattice parameters (a, b, c, and β), bandgap E_{gap}, and formation energy ΔH_f of β-Ga_2O_3 obtained from our calculations, HSE06 results reported in the literature, and experimental measurements (Expt.).

Parameter	This work	HSE06	Expt.
a (Å)	12.20	12.23[a]	12.214[d]
b (Å)	3.03	3.03[a]	3.037[d]
c (Å)	5.78	5.79[a]	5.798[d]
β (deg)	103.8	103.9[b]	103.8[d]
E_{gap} (eV)	4.9	4.9[a]	4.9[e]
$\Delta H_f(\beta\text{-}Ga_2O_3)$ (eV)	−12.7	−10.3[c]	−11.3[f]

[a] Ref. [21]; [b] Ref. [22]; [c] Ref. [23] ; [d] Ref. [24] ; [e] Ref. [25]; [f] Ref. [26].

2. Method

In this work, all the first-principles calculations were performed using the PWMAT[16, 17] package with the SG15 collection of the optimized norm-conserving Vanderbilt pseudopotentials (ONCV)[18] with an energy cutoff of 70 Ryd. Heyd-Scuseria-Ernzerhof (HSE)[19] screened hybrid functional was applied for all the calculations except the calculations of electron-phonon coupling constants which used the Perdew-Burke-Ernzerhof functional of the generalized gradient approximation (GGA-PBE). The Ga-4*s*, -4*p*, Ti-3*s*, 3*p*, -3*d*, -4*s*, and Fe-*3s*, -*3p*, -*3d*, -*4s* electrons were included as valence electrons. The fraction of the screened Hartree-Fock exchange was adjusted to $\alpha = 0.33$ to reproduce the experimental band gap of 4.9 eV. The lattice parameters of the pure β-Ga_2O_3 were predicted to be $a = 12.20$ Å, $b = 3.03$ Å, and $c = 5.78$ Å with $\beta = 103.8$, as shown in Table 2. A 160-atom ($1\times4\times2$) supercell is adopted to calculate defects with a Gamma-only k-point mesh for integration over the Brillouin zone. Fig. 1 shows the atomic configuration of one Ti substituting one Ga atom on the tetrahedral site (Ti_{GaI}) and the octahedral site (Ti_{GaII}), respectively, in β-Ga_2O_3. The defect of Fe substitution of Ga (Fe_{Ga}) has the same configurations as Ti_{Ga} except for the replacement of Ti by Fe. We have considered spin polarization for the incorporation of Fe ions in the first-principles calculations. Fe substituting Ga atom in +3 $\left(S=\frac{5}{2}\right)$ and +2 ($S = 2$) states[8, 20] are labeled as Fe^0_{Ga} and Fe^-_{Ga}.

We use a well-established set of approaches[27, 28] to calculate the formation energies and transition levels $\varepsilon_{i/f}$ of the defects based on the first-principles calculations of total energy. Specifically, for charged defects, we utilize the image charge interaction correction with the approximation method (C-AP) proposed in Ref. [29] to obtain the defect formation

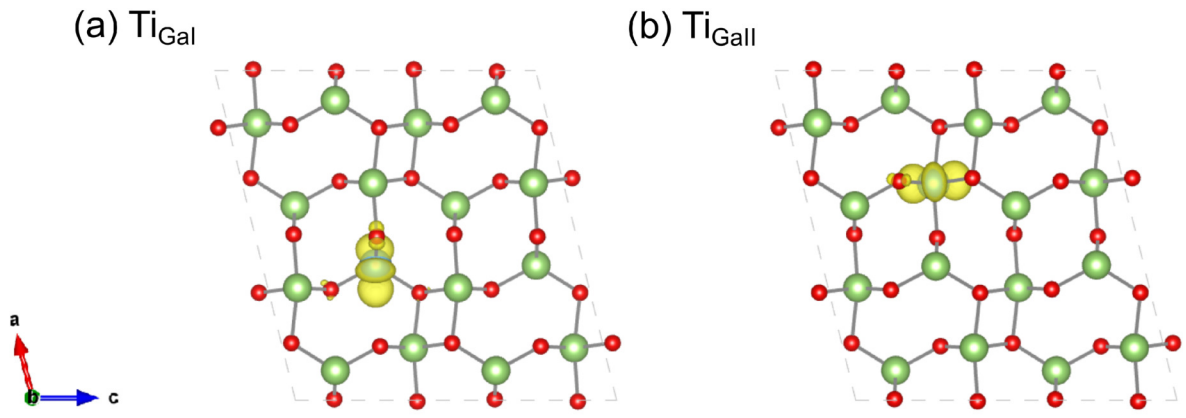

Fig. 1. (Color online) The partial charge density of the defect states of (a) Ti_{GaI} (substitute on the tetrahedral site) and (b) Ti_{GaII} (substitute on the octahedral site) defects in β-Ga_2O_3.

energy as follows,

$$\Delta H_f(\alpha, q) = \{E(\alpha, q) + E_C(\alpha, q)\} - E(\text{host}) - \sum_i n_i\mu_i + q(\varepsilon_F + \varepsilon_{VBM}). \quad (1)$$

Here, $E(\alpha, q)$ is the total energy of a supercell containing the defect α in a charge state q, $E_C(\alpha, q)$ is the C-AP correction term, E(host) is the total energy of the bulk host supercell without defect, and n_i is the number of atoms with chemical potential μ_i added ($n_i > 0$) to or removed ($n_i < 0$) from the supercell to create the defect. The chemical potential of Ga(μ_{Ga}) is in a range with its upper and lower bound setting by bulk elemental Ga (Ga-rich) and the stability condition of Ga_2O_3 (Ga-poor), respectively. The chemical potential of Fe(μ_{Fe}) is in a range determined by Ga_3Fe and Fe_2O_3[8] and μ_{Ti} is determined by TiO_2. The Fermi level ε_F is referenced to$\varepsilon_{VBM}$the valence band maximum (VBM) of the host (here is Ga_2O_3) with its potential aligned with the potential of defect supercell at the corner (farthest away from the defect). The transition level from the initial state i in a charge state q to the final state f in a charge state q' is the difference of their formation energy per charge when their Fermi levels equal,

$$\varepsilon_{i/f} = \frac{\Delta H(\alpha, q, E_F = 0) - \Delta H(\alpha, q', E_F = 0)}{q' - q}. \quad (2)$$

For the transition levels $\varepsilon_{i/f}$ close to the CBM, we transform them to referring to the CBM in terms of $\varepsilon_{i/f}$(CBM) = E_g–$\varepsilon_{i/f}$(VBM).

To calculate the nonradiative carrier capture cross-sections of defects, we then utilize the recently developed *ab initio* multi-phonon method for nonradiative decay rates[30–33] based on the multi-phonon recombination theory from Kun Huang[34–36], which has been implemented in the PWMAT[16, 17] package. Specifically, the nonradiative decay probability from the initial electronic state i to the final electronic state f is[30]

$$W_{if} = \frac{1}{\hbar}\left(\frac{\pi}{\lambda k_B T}\right)^{1/2} \sum_k \frac{k_B T}{\omega_k^2}\left(\sum_R \langle i|\frac{\partial H}{\partial R}|f\rangle \mu_k(R)\right)^2 e^{-\frac{(\varepsilon_{i/f}-\lambda)^2}{4\lambda k_B T}}, \quad (3)$$

where $\varepsilon_{i/f}$ is the defect transition level measured from CBM, λ the reorganization energy induced by the electron transfer from i to f states, and $\mu_k(R)$ the eigenvector of the phonon modes. The corresponding coordinate difference ΔQ can be obtained in terms of $\Delta Q = \sqrt{\sum_\alpha M_\alpha \Delta R_\alpha^2}$, where α is atom index in the supercell, M_α is the nuclear mass, and $\Delta R_\alpha = R_{f;\alpha} - R_{i;\alpha}$ the atomic displacement. The summation term in Eq. (3) is defined as an electron-phonon coupling constant $|V_C|^2 = \sum_k \frac{k_B T}{\omega_k^2}\left(\sum_R \langle i|\frac{\partial H}{\partial R}|f\rangle \mu_k(R)\right)^2$, which indicates that the perturbation ΔH caused by atomic displacement due to random thermal vibrations can induce coupling between electronic states i and j[30]. Once we get the nonradiative recombination probability W_{if} according to Eq. (3), we can further compute the carrier capture rate coefficient $B = W_{if}V$ (where V is the volume of the supercell), which is divided by the average thermal velocity $v_{th} = \sqrt{3k_BT/m^*}$ (where k_B is Boltzmann constant, T is temperature, and m^* is the carrier effective mass) to finally obtain the carrier capture cross-section $\sigma = B/v_{th}$. In β-Ga_2O_3, the electron effective mass is $m^* \approx 0.23m_0$[37] and thus, at temperature T = 300 K, v_{th} is 2.44 × 10^7 cm/s, which is very close to the reported electron velocity of ~2 × 10^7 cm/s in Ref. [38].

3. Results and discussion

We have considered the substitutions of Ga atom on both tetrahedral (Ti_{GaI} and Fe_{GaI}) and octahedral sites (Ti_{GaII} and Fe_{GaII}). To investigate the capture of electrons by defect levels, we study the +/0 charge transition for Ti_{Ga} and 0/– transition for Fe_{Ga}. Our first-principles calculated transition levels and electron capture cross-sections of Ti_{Ga} and Fe_{Ga} defects are given in Table 3, in comparison with available results reported in the literature. Our calculated defect levels $\varepsilon_{+/0}$ of Ti_{GaI} and Ti_{GaII} are 0.59 and 1.08 eV (below the CBM of β-Ga_2O_3), within the range of ~0.05 eV of previously reported first-principles calculations (0.60 and 1.13 eV for Ti_{GaI} and Ti_{GaII}, respectively)[10]. For Fe_{GaI} and Fe_{GaII}, our predicted transition levels $\varepsilon_{0/-}$ are 0.61 and 0.74 eV below the CBM, respectively. They are in excellent agreement with previously reported first-principles results, 0.62 and 0.72 eV[17], respectively. It is ready to learn that both the Ti_{Ga} and Fe_{Ga} defects presenting at the Ga octahedral site (GaII) have deeper energy levels than those at the Ga tetrahedral site (GaI). To assess the trapping center assignment based on defect levels, we align our calculated Ti_{Ga}

Table 3. First-principles calculated results of Ti_{Ga} and Fe_{Ga} defects in β-Ga_2O_3. The transition levels $\varepsilon_{i/f}$ and the configuration difference ΔQ are in comparison with those reported in the literature. Reorganization energies λ, electron-phonon coupling constants $|V_C|^2$, and electron capture cross-sections σ_n of Ti_{Ga} and Fe_{Ga} are included.

Parameter	Defect	Ti_{Gal}	Ti_{GaII}	Fe_{Gal}	Fe_{GaII}
$\varepsilon_{i/f}$ (eV)	Cal.	(+/0) 0.59	(+/0) 1.08	(0/–) 0.61	(0/–) 0.74
	Refs. [10, 11]	0.60	1.13	0.62	0.72
ΔQ (amu$^{1/2}$/Å)	Cal.	2.06	1.42	1.61	1.32
	Refs. [10, 11]	~2.0	1.35	1.63	1.22
λ (eV)	$E_{ji} - E_{ii}$	1.06	0.81	0.76	0.70
$\|V_C\|^2$ (eV^2)	Cal. 300 K	0.58	0.56	0.43	0.48
σ_n (cm^2)	Cal. 300 K	8.56×10^{-14}	2.97×10^{-13}	4.23×10^{-13}	6.42×10^{-13}

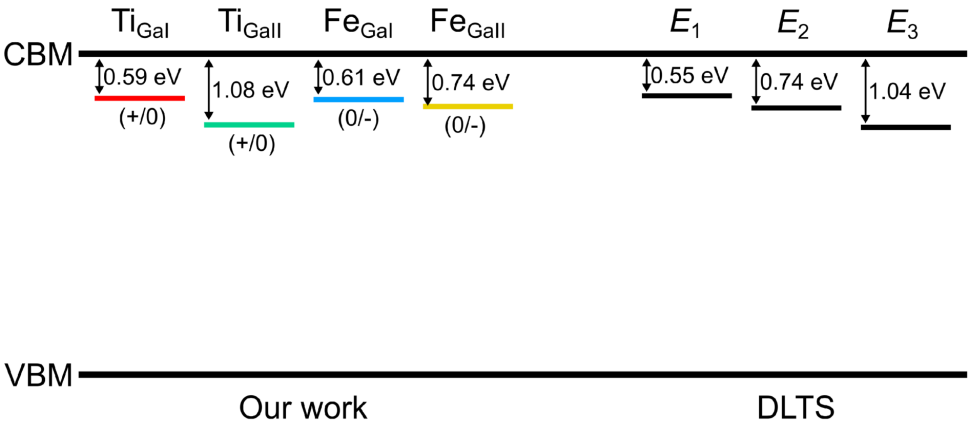

Fig. 2. (Color online) The defect transition levels of Ti_{Ga} and Fe_{Ga} in β-Ga_2O_3 predicted by the first-principles calculations compared with the defect signatures E_1, E_2, E_3 observed in DLTS measurements[4]. All energy levels are referenced to the CBM, which is 4.9 eV above the VBM and gives rise to β-Ga_2O_3 a bandgap of 4.9 eV.

and Fe_{Ga} defect transition levels with the DLTS measured defect signatures E_1, E_2, E_3, as shown in Fig. 2. From the alignment of energy levels alone, we indeed see that Ti_{Gal}, Fe_{GaII}, and Ti_{GaII} can be correlated with E_1, E_2, and E_3 trapping centers, respectively, which is consistent with previous assignments[8, 10].

Based on the calculated transition levels $\varepsilon_{i/f}$ given in Table 3, we then predicted the electron capture cross-sections σ_n of Ti_{Gal} and Ti_{GaII} defects at 300 K by performing the first-principles calculations according to Eq. (3). Table 3 shows that σ_n of Ti_{Gal} is 8.56×10^{-14} cm^2 and of Ti_{GaII} is 2.97×10^{-13} cm^2. These two data are well within the range 10^{-14}–10^{-13} cm^2 of experimental data of E_1 and E_3 centers (compiled in Table 1)[4, 5, 7]. Note that these are cross-sections for electron trapping from the original positive defect and hence could have a correction factor due to the long-range Coulomb interaction between defect and electron[39], which makes the concentration of the electron carriers near the defect larger than the average carrier density. The exact value of this correction factor depends on many factors, including the static dielectric function, the carrier concentration, the carrier effective mass, and temperature. In previous studies[39], this factor was found to be within 1 and 10 for oxides. After considering this correction factor, these calculated decay cross-sections for Ti_{Gal} and Ti_{GaII} are still within the experimental range of E_1 and E_3 centers. Based on this, we thus conclude that the atomic origin of the E_1 trapping center is Ti_{Gal} and the E_3 trapping center is Ti_{GaII}. Whereas Table 3 shows that the electron capture cross-sections σ_n of Fe_{Gal} and Fe_{GaII} at 300 K are 4.23×10^{-13} and 6.42×10^{-13} cm^2, respectively. Note, for the initial neutral defect, the above-mentioned correction factor is close to 1. Therefore, the electron capture cross-sections of Fe_{Gal} and Fe_{GaII} defects are at least two orders of magnitude larger than the experimental value of 10^{-16}–10^{-15} cm^2 for E_2 center[4, 5, 7]. Such substantial disagreement in the electron capture cross-section rules out the Fe_{Ga} defect as the E_2 center, although from the energy level comparison we can assign Fe_{GaII} as the E_2 center or Fe_{Gal} and Fe_{GaII} as the E_{2a} and E_{2b} levels, respectively.

Nevertheless, before overturning the previous assignment for the E_2 center[8, 10], it is necessary to examine whether the computational uncertainties in the transition level and the coupling term can cause such a big disagreement in the electron capture cross-section between the E_2 center and its candidate Fe_{Ga}. First, the calculated coordinate difference ΔQ in the charge transitions are 2.06 (Ti_{Gal}), 1.42 (Ti_{GaII}), 1.61 (Fe_{Gal}), and 1.32 (Fe_{GaII}) amu$^{1/2}$/Å respectively, which are consistent with the previous first-principles calculations presented in Refs. [10, 11]. This confirms that our supercell configurations and energy level calculations are aligned with the literature.

We then inspect the effect of energy level uncertainty on the electron capture cross-sections of defect candidates. Fig. 3 shows the calculated electron capture cross-sections σ_n of Ti_{Ga} and Fe_{Ga} as a function of the defect transition level $\varepsilon_{i/f}$ at 300 K, which is an artificially rigid shift inside the host Ga_2O_3 bandgap from VBM to CBM. σ_n of Ti_{Ga} and Fe_{Ga} changes from ~10^{-19} to ~10^{-12} when $\varepsilon_{i/f}$ varies from ~2.4 eV

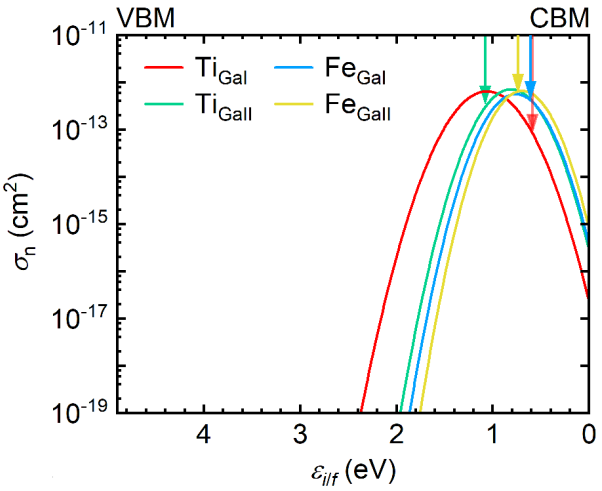

Fig. 3. (Color online) First-principles-calculated σ_n as a function of the transition level $\varepsilon_{i/f}$ for TiGa and FeGa at 300 K. The vertical arrows pointed out the σ_n using the calculated transition levels $\varepsilon_{i/f}$ in Table 3. The energy is referenced to the CBM which is 0 eV.

below CBM to CBM. Note that the peak position corresponding to the reorganization energy λ can also be written down as $S\overline{\hbar\omega}_k$[30] with the Huang-Rhys' factor S[35, 36]. At the peak position, W_{if} and σ_n will get the maximum value because the defect level $\varepsilon_{i/f}$ equals the reorganization energy λ and then $\exp\left(-\frac{(\varepsilon_{i/f}-\lambda)^2}{4\lambda k_B T}\right) = 1$. As we can see, the maximum σ_n for these defects are almost at the same magnitude, so σ_n for each defect is finally determined by the exponential term, more specifically the energy difference between $\varepsilon_{i/f}$ and λ. Table 3 shows the transition level $\varepsilon_{i/f}$ of defects is very close to its reorganization energy, except for Ti_{GaI} whose $\varepsilon_{i/f}$ is ~0.5 eV lower than λ. Thus, the carrier capture cross-sections σ_n are relatively high for the Ti_{GaII}, Fe_{GaI}, and Fe_{GaII} defects, mostly in the magnitude of 10^{-13} at 300 K, while σ_n of Ti_{GaI} is a little smaller. These are relatively strong trappings of electrons and indicate the importance of these defects for carrier dynamics. In comparison, the defects in another typical wide-bandgap semiconductor SiC have much smaller trapping rates; for example, the electron capture cross-sections of defects such as V_C, V_{Si}, V_C–V_{Si}, and N_C–V_{Si} in 4H-SiC are all less than the order of 10^{-15}[3]. Fig. 3 shows the dependence of σ_n on $\varepsilon_{i/f}$ for each defect shares the same variation tendency and shape, indicating that the differences induced by the transition metal atoms Ti and Fe can be small. Thus, σ_n of Ti_{Ga} and Fe_{Ga} are in a similar order of magnitude.

We finally examine the effect of the electron-phonon coupling term $|V_C|^2$ for the capture cross-sections via comparing Fe_{Ga} and Ti_{Ga} defects. Table 3 shows that $|V_C|^2$ for Ti_{GaI} and Ti_{GaII} defects are 0.58 and 0.56 eV^2, respectively, and for Fe_{GaI} and Fe_{GaII} defects are 0.43 and 0.48 eV^2, respectively. The difference between two nonequivalent sites is tiny for each defect and the difference between Ti_{Ga} and Fe_{Ga} is also small. To gain insight into their similarity in the magnitude of $|V_C|^2$, we further evaluate the phonon mode and wavefunction of the defects, which govern the electron-phonon coupling constant $|V_C|^2$. Fig. 4(a) shows the phonon density of states (ph-DOS) for the system containing Ti_{GaI} and Ti_{GaII}, respectively. One can find that the different substituting sites will not induce a sizable change in the ph-DOS. This is also true for the Fe_{Ga} defect as shown in Fig. 4(b). It is even more interesting to note that the Fe_{Ga} defects resemble their ph-DOS with Ti_{Ga} defects, indicating the change in the impurity atom seldom affects the ph-DOS of the system. One main factor is that they have similar ionic radius due to Fe and Ti. In the 6-fold coordination configuration, the ionic radius of the Ti impurity changes from 0.68 to 0.76 Å from Ti^{4+} to Ti^{3+}, and the ionic radius of the Fe impurity changes from 0.64 to 0.74 Å from Fe^{3+} to Fe^{2+}[40]. As for the electronic property, Fig. 1 shows that the partial charge densities of the Ti_{GaI} and Ti_{GaII} defect states are very similar because they both originate from the Ti 3*d* orbitals. It is also expected to be the same in the Fe_{Ga} defects where the defect states stem from the Fe 3*d* orbitals. Subsequently, the effective phonon modes involving the electron-phonon coupling are also similar, even though there may have small differences in strength among these four defects, as shown in Figs. 4(c)–4(f). These above features result in the close $|V_C|^2$ for Ti_{GaI} and Ti_{GaII}, as well as for Fe_{GaI} and Fe_{GaII}. The change from Ti to Fe is unlike to remarkably alter the $|V_C|^2$.

Although the reorganization energy λ of these defects varies from 0.7 to 1.06 eV as listed in Table 3, Fig. 3 shows that, for all the defects, the maximum of W_{if} at $\varepsilon_{i/f} = \lambda$ are in the same order of magnitude, which are 0.94×10^{16}, 1.04×10^{16}, 0.83×10^{16}, and 0.97×10^{16} s^{-1} for Ti_{GaI}, Ti_{GaII}, Fe_{GaI}, and Fe_{GaII}, respectively. The similarities in the ph-DOS, the defect charge density from the 3*d* orbital, and the similar impurity ion radius all contribute to the above similarity for the maximum capture rate. The similarity of the maximum W_{if} and the fact that their transition level energy is close to the reorganization energy λ result in a similar magnitude of σ_n around 10^{-13} cm^2 for Fe_{Ga} and Ti_{Ga} defects. Based on this analysis, it is clear that Fe_{Ga} and Ti_{Ga} cannot have dramatically different σ_n. Even if there are some computational uncertainties, these uncertainties should equally apply to both Fe_{Ga} and Ti_{Ga}. We have concluded Ti_{GaI} and Ti_{GaII} are responsible for E_1 and E_3, respectively. Thus, the apparent difference (two orders of magnitude) in experimentally measured σ_n between E_1 (or E_3) and E_2 might be used as evidence for excluding Fe_{Ga} from the assignment to E_2.

From the perspective of the defect formation energy, we can also argue that the Fe_{Ga} defects are relatively unlike to form due to their high formation energy. Note that β-Ga_2O_3 is generally an n-type semiconductor. Fig. 5 exhibits that, to form the Ti_{Ga} (E_1 and E_3) defects clearly, the system must be in an O-poor condition (otherwise, the Ti_{Ga} formation energy can be as high as 2–3 eV). Under this O-poor condition, the literature has reported that the formation energies of both Fe_{GaI} and Fe_{GaII} are always higher than both Ti_{GaI} and Ti_{GaII}[8, 10]. Our calculations also show that the formation energy of Fe_{Ga} is higher than that of Ti_{Ga} if the Fermi level is ~0.8 eV below the CBM. The difference occurs only in the case of high n-type doping. Fig. 5(a) shows that the formation energy of Ti_{GaI} will raise over those of both Fe_{GaI} and Fe_{GaII}, while Ti_{GaII} remains smaller than the formation energy as the Fermi level increases towards CBM due to heavier n-type doping, which argues for the unfavorable formation of Fe_{Ga}. Experimental measurements have observed[41] that electron trapping centers E_2 and E_3 have a comparable concentration of $(2–4) \times 10^{16}$ cm^{-3}, but E_1 has one order of magnitude lower concentration (3 ×

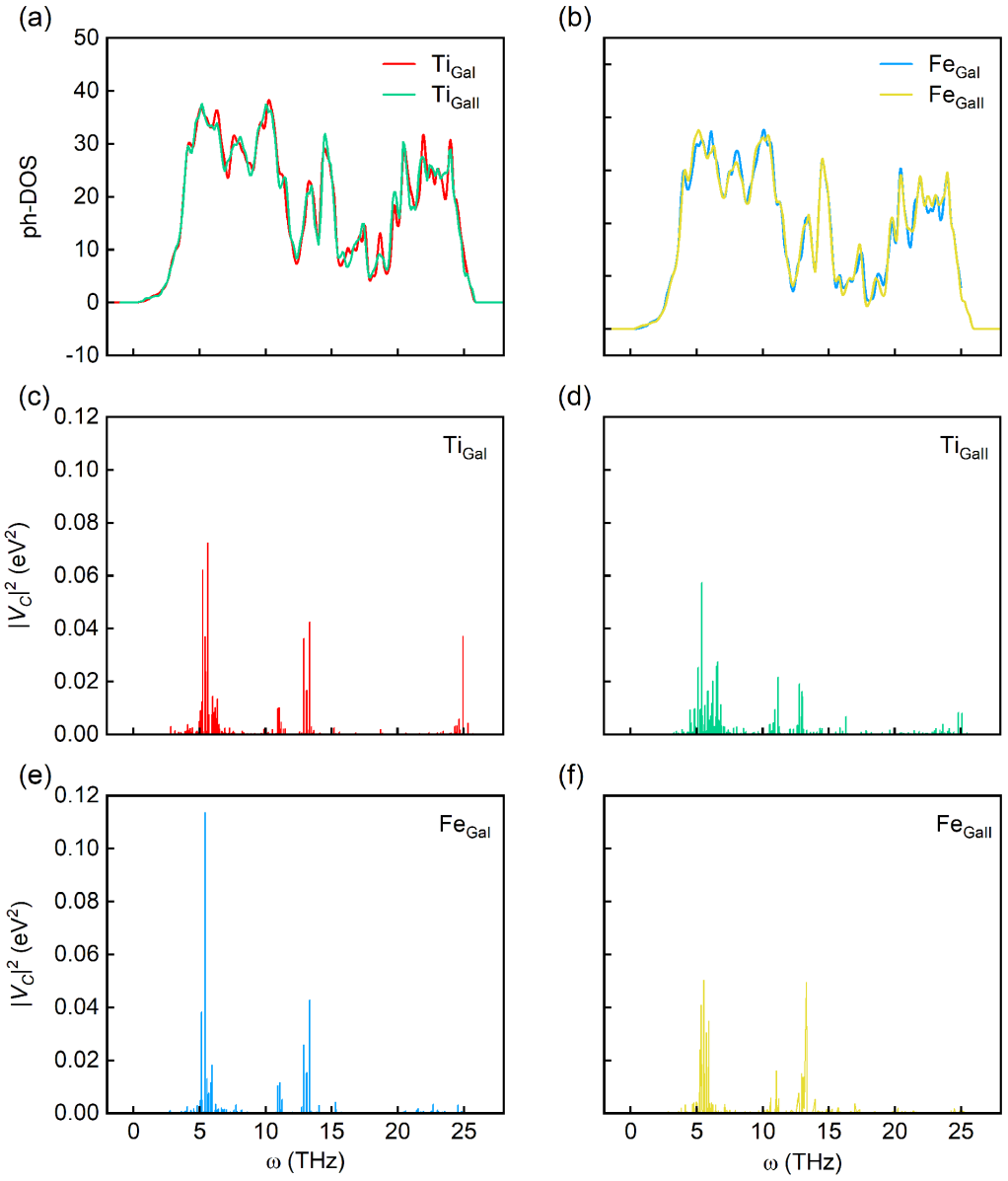

Fig. 4. (Color online) Items in $|V_C|^2$ for Ti_{Ga} and Fe_{Ga} defects. Ph-DOS as a function of phonon frequency for the supercell containing (a) Ti_{Ga} and (b) Fe_{Ga}. The coupling constant $|V_C|^2$ as a function of phonon frequency in the electron-phonon coupling with (c) Ti_{GaI}, (d) Ti_{GaII}, (e) Fe_{GaI}, and (f) Fe_{GaII}.

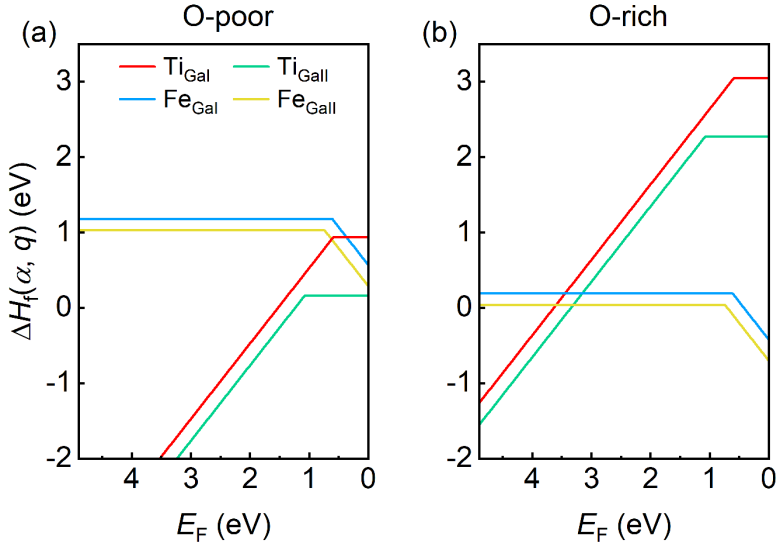

Fig. 5. (Color online) The formation energy of Ti_{Ga} and Fe_{Ga} defects as a function of Fermi level under (a) O-poor conditions and (b) O-rich conditions. The Fermi energy is referenced to CBM which is set to 0 eV.

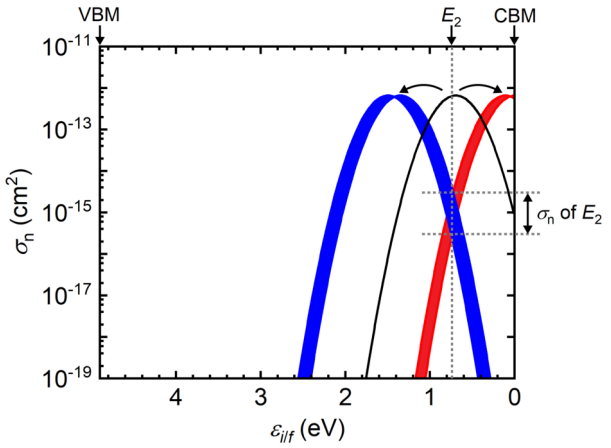

Fig. 6. (Color online) Schematic diagram for $\sigma_n(\varepsilon_{i/f})$ of E_2 candidates with proper reorganization energy λ. $\varepsilon_{i/f}$ is referenced to CBM which is 0 eV at the right of the horizontal axis. The experimental defect level of E_2 is 0.74 eV[4] below the CBM, shown as the vertical dotted line. The horizontal dotted lines indicate the minimum and maximum experimental σ_n ($(0.3–3) \times 10^{-15}$ cm^2[4]) of E_2. For the candidates, the downward "parabola" is intrinsic and the maximum σ_n remains still (see the black curve which is for Fe_{GaII} from Fig. 3), while the reorganization energy can be adjusted through shifting the "parabola" curve left (increasing λ) and right (decreasing λ). Meanwhile, σ_n of the blue and red curves at 0.74 eV should be within the experimental range, σ_n of E_2, to give the reorganization energy at ~1.4 eV (left shifting) and ~0.1 eV (right shifting), respectively.

10^{14}–6×10^{15} cm^{-3})[41]. Our predicted higher formation energy of Ti_{GaI} (E_1) than that of Ti_{GaII} (E_3), as shown in Fig. 5(a), clearly explains the concentration difference between E_1 and E_3 centers. However, the high formation energy of Fe_{Ga} (E_2) renders it impossible to have a comparable high concentration as Ti_{GaII} (E_3). Subsequently, we can safely rule out the Fe_{Ga} defects as the atomic origin of the E_2 center, which is the dominant electron trapping center and presents in all β-Ga_2O_3 samples.

Since we have ruled out the assignment of Fe_{Ga} as the E_2 center, it must have other defects responding to it. For instance, Irmscher *et al.*[4] postulated that E_2 may be associated with Sn_{Ga} and V_O; Farzana *et al.*[5] proposed C-related origins. From our understanding, we can suggest the possible E_2 candidates. We have mentioned above that the electron capture cross-sections of deep level defects in β-Ga_2O_3 are at least an order of magnitude larger than those in SiC. Because SiC is more covalent than β-Ga_2O_3, thus results in a weaker lattice vibration-induced local dipolar field and electron-phonon coupling. Hence, we expect the change of foreign atoms is unlikely to substantially change the maximum value of σ_n at $\varepsilon_{i/f} = \lambda$. However, we can horizontally shift the downward "parabola" of the $\sigma_n(\varepsilon_{i/f})$ by modifying the reorganization energy λ, as shown in Fig. 6, to remarkably reduce the σ_n value at $\varepsilon_{i/f} = E_2$. Fig. 6 shows the schematic diagram for $\sigma_n(\varepsilon_{i/f})$ of E_2 candidates with proper reorganization energy λ. Here, an experimental defect level of E_2 (0.74 eV[4]) is adopted, and the experimental electron capture cross-section σ_n is $(0.3–3) \times 10^{-15}$ cm^2[4] . These two conditions require the candidates to have the reorganization energy at ~1.4 or ~0.1 eV. This means the large atom size difference between substituting atom and the host lattice atom or even complex defects can induce strong local distortion, resulting in a large reorganization energy of ~1.4 eV. Meanwhile, a defect with very small reorganization energy as ~0.1 eV, meaning the less atom size difference and weak local distortion, may also make sense. The first-principles calculation predicted transition level of the C_{Ga} defect is 0.81 eV below CBM[42] which is very close to the E_2 level of 0.74 eV. The large difference in atom size between C and Ga is expected to induce strong distortion, which may give rise to larger reorganization energy (as large as ~1.4 eV) than 0.70 eV of Fe_{GaII} and have $\sigma_n(\varepsilon_{i/f})$ curve like the blue one shown in Fig. 6. Therefore, C_{Ga} is very likely responsible for E_2. However, the defect level of V_O is 1.67–2.46 eV below CBM[13], rather deeper than 0.74 eV; Sn_{Ga} has the defect level of 0.19 eV below CBM[42] which is too shallow. Both V_O and Sn_{Ga} are unlikely responsible for the E_2 center. Beyond these defects suggested in the literature, we find that Ga_i and Ga_{OII}[7], V_{Ga}–V_O divacancies such as V_{GaII}–V_{OI} or V_{GaI}–V_{OII}[21] all have the defect levels at 0.7–0.9 eV below CBM and may also induce strong distortion and have large reorganization energy. Subsequently, the C_{Ga}, Ga_i, Ga_{OII}, and V_{Ga}–V_O defects can be candidates for E_2 and need to be studied further in the future.

4. Conclusion

We use first-principles methods to calculate the defect levels and the electron capture cross-sections of Ti_{Ga} and Fe_{Ga} in β-Ga_2O_3 which have been assigned to the experimental signatures E_1, E_3, and E_2 centers in the literature. Using both transition level position and electron capture cross-sections as criteria, we proposed that Ti substituting for Ga on a tetrahedral site (Ti_{GaI}) and an octahedral site (Ti_{GaII}) are indeed associated with E_1 and E_3 states respectively. However, for the signature level E_2, the Fe substituting for Ga on a tetrahedral and an octahedral site have calculated transition level energies in good agreement with the experiment, but the calculated electron capture cross-sections are two orders of magnitude larger than the experimental results. A comparative analysis between the Ti_{Ga} and Fe_{Ga} defects and a computational sensitivity study of electron capture cross-sections indicate that the computational uncertainty is unlikely to cause a two order of magnitude difference in the electron capture cross-sections between Ti_{Ga} and Fe_{Ga}. Besides, the calculated formation energy shows it is unfavorable for the Fe_{Ga} formation. All of these lead us tentatively exclude Fe_{Ga} as the experimentally observed E_2 signature. Thus, the exact nature of E_2 awaits future experimental and theoretical discovery.

Acknowledgements

Zhaojun Suo acknowledges the fruitful discussions with Yuxiang Gu. This work was supported by the National Key Research and Development Program of China under Grant No. 2018YFB2200105, the Key Research Program of Frontier Sciences, CAS under Grant No. ZDBS-LY-JSC019, and the National Natural Science Foundation of China (NSFC) under Grant Nos. 11925407 and 61927901.

References

[1] Pearton S J, Yang J C, Cary P H IV, et al. A review of Ga_2O_3 materials, processing, and devices. Appl Phys Rev, 2018, 5, 011301

[2] Higashiwaki M, Sasaki K, Murakami H, et al. Recent progress in Ga_2O_3 power devices. Semicond Sci Technol, 2016, 31, 034001

[3] Gu Y X, Shi L, Luo J W, et al. Directly confirming the $Z_{1/2}$ center as the electron trap in SiC through accessing the nonradiative recombination. Phys Status Solidi R, 2022, 16, 2100458
[4] Irmscher K, Galazka Z, Pietsch M, et al. Electrical properties of β-Ga_2O_3 single crystals grown by the Czochralski method. J Appl Phys, 2011, 110, 063720
[5] Farzana E, Chaiken M F, Blue T E, et al. Impact of deep level defects induced by high energy neutron radiation in β-Ga_2O_3. APL Mater, 2019, 7, 022502
[6] Polyakov A Y, Smirnov N B, Shchemerov I V, et al. Compensation and persistent photocapacitance in homoepitaxial Sn-doped β-Ga_2O_3. J Appl Phys, 2018, 123, 115702
[7] Ingebrigtsen M E, Kuznetsov A Y, Svensson B G, et al. Impact of proton irradiation on conductivity and deep level defects in β-Ga_2O_3. APL Mater, 2019, 7, 022510
[8] Ingebrigtsen M E, Varley J B, Kuznetsov A Y, et al. Iron and intrinsic deep level states in Ga_2O_3. Appl Phys Lett, 2018, 112, 042104
[9] Polyakov A Y, Smirnov N B, Shchemerov I V, et al. Point defect induced degradation of electrical properties of Ga_2O_3 by 10 MeV proton damage. Appl Phys Lett, 2018, 112, 032107
[10] Zimmermann C, Frodason Y K, Barnard A W, et al. Ti- and Fe-related charge transition levels in β-Ga_2O_3. Appl Phys Lett, 2020, 116, 072101
[11] Zimmermann C, Kalmann Frodason Y, Rønning V, et al. Combining steady-state photo-capacitance spectra with first-principles calculations: The case of Fe and Ti in β-Ga_2O_3. New J Phys, 2020, 22, 063033
[12] Polyakov A Y, Smirnov N B, Shchemerov I V, et al. Defects responsible for charge carrier removal and correlation with deep level introduction in irradiated β-Ga_2O_3. Appl Phys Lett, 2018, 113, 092102
[13] Zimmermann C, Rønning V, Kalmann Frodason Y, et al. Primary intrinsic defects and their charge transition levels in β-Ga_2O_3. Phys Rev Mater, 2020, 4, 074605
[14] Lee M H, Peterson R L. Interfacial reactions of titanium/gold ohmic contacts with Sn-doped β-Ga_2O_3. APL Mater, 2019, 7, 022524
[15] Zhang Z, Farzana E, Arehart A R, et al. Deep level defects throughout the bandgap of (010) β-Ga_2O_3 detected by optically and thermally stimulated defect spectroscopy. Appl Phys Lett, 2016, 108, 052105
[16] Jia W L, Fu J Y, Cao Z Y, et al. Fast plane wave density functional theory molecular dynamics calculations on multi-GPU machines. J Comput Phys, 2013, 251, 102
[17] Jia W L, Cao Z Y, Wang L, et al. The analysis of a plane wave pseudopotential density functional theory code on a GPU machine. Comput Phys Commun, 2013, 184, 9
[18] Hamann D R. Optimized norm-conserving Vanderbilt pseudopotentials. Phys Rev B, 2013, 88, 085117
[19] Heyd J, Scuseria G E, Ernzerhof M. Hybrid functionals based on a screened Coulomb potential. J Chem Phys, 2003, 118, 8207
[20] Bhandari S, Zvanut M E, Varley J B. Optical absorption of Fe in doped Ga_2O_3. J Appl Phys, 2019, 126, 165703
[21] Frodason Y K, Zimmermann C, Verhoeven E F, et al. Multistability of isolated and hydrogenated Ga-O divacancies in β-Ga_2O_3. Phys Rev Materials, 2021, 5, 025402
[22] Varley J B, Weber J R, Janotti A, et al. Oxygen vacancies and donor impurities in β-Ga_2O_3. Appl Phys Lett, 2010, 97, 142106
[23] Zacherle T, Schmidt P C, Martin M. *Ab initio* calculations on the defect structure of β-Ga_2O_3. Phys Rev B, 2013, 87, 235206
[24] Åhman J, Svensson G, Albertsson J. A reinvestigation of β-gallium oxide. Acta Crystallogr C, 1996, 52, 1336
[25] Orita M, Ohta H, Hirano M, et al. Deep-ultraviolet transparent conductive β-Ga_2O_3 thin films. Appl Phys Lett, 2000, 77, 4166
[26] Thermochemical Data of Pure Substances. Part I + II. Von I. Barin. VCH Verlagsgesellschaft, Weinheim/VCH Publishers, New York 1989. Part I: I-1 – I 87, S. 1–816; Part II: VI, S. 817–1739; Geb. DM 680.00.— ISBN 3-527-27812-5/0-89573-866-X - Maier=1990-Angewandte Chemie-Wiley Online Library, https://onlinelibrary.wiley.com/doi/abs/10.1002/ange.19901020738
[27] Freysoldt C, Grabowski B, Hickel T, et al. First-principles calculations for point defects in solids. Rev Mod Phys, 2014, 86, 253
[28] Wei S H. Overcoming the doping bottleneck in semiconductors. Comput Mater Sci, 2004, 30, 337
[29] Suo Z J, Luo J W, Li S S, et al. Image charge interaction correction in charged-defect calculations. Phys Rev B, 2020, 102, 174110
[30] Xiao Y, Wang Z W, Shi L, et al. Anharmonic multi-phonon nonradiative transition: An *ab initio* calculation approach. Sci China Phys Mech Astron, 2020, 63, 277312
[31] Shi L, Wang L W. *Ab initio* calculations of deep-level carrier nonradiative recombination rates in bulk semiconductors. Phys Rev Lett, 2012, 109, 245501
[32] Shi L, Xu K, Wang L W. Comparative study of *ab initio* nonradiative recombination rate calculations under different formalisms. Phys Rev B, 2015, 91, 205315
[33] Wang L W. Some recent advances in *ab initio* calculations of nonradiative decay rates of point defects in semiconductors. J Semicond, 2019, 40, 091101
[34] Huang K. On the applicability of adiabatic approximation in multiphonon recombination theory. J Semicond, 2019, 40, 090102
[35] Zhang Y. Applications of Huang-Rhys theory in semiconductor optical spectroscopy. J Semicond, 2019, 40, 091102
[36] Huang K, Rhys A. Theory of light absorption and non-radiative transitions in *F*-centres. Proc R Soc Lond A, 1950, 204, 406
[37] Yamaguchi K. First principles study on electronic structure of β-Ga_2O_3. Solid State Commun, 2004, 131, 739
[38] Mastro M A, Kuramata A, Calkins J, et al. Perspective—opportunities and future directions for Ga_2O_3. ECS J Solid State Sci Technol, 2017, 6, P356
[39] Alkauskas A, Yan Q M, van de Walle C G. First-principles theory of nonradiative carrier capture via multiphonon emission. Phys Rev B, 2014, 90, 075202
[40] Ahrens L H. The use of ionization potentials Part 1. Ionic radii of the elements. Geochim Cosmochim Acta, 1952, 2, 155
[41] Zhang J Y, Shi J L, Qi D C, et al. Recent progress on the electronic structure, defect, and doping properties of Ga_2O_3. APL Mater, 2020, 8, 020906
[42] Lany S. Defect phase diagram for doping of Ga_2O_3. APL Mater, 2018, 6, 046103

Zhaojun Suo is a Ph.D. candidate at the Institute of Semiconductors CAS, under the supervision of Professor Junwei Luo. Her research focuses on semiconductor defect calculation and related methods, and laser-induced phase transition.

Linwang Wang got his Ph.D. from Cornell University. After postdoctoral work at Cornell University and National Renewable Energy Laboratory, he worked at National Renewable Energy Laboratory and Lawrence Berkeley National Laboratory. He is a chief scientist at the Institute of Semiconductors CAS. His research focuses on the development of first-principles methods and software packages in semiconductor materials, new energy materials, or related devices.

Junwei Luo received his Ph.D. from the Institute of Semiconductors CAS in 2007. He was then appointed as a postdoc fellow, scientist, and senior scientist at the U.S. DOE's National Renewable Energy Laboratory (NREL). He returned to the Institute of Semiconductors as a professor in 2014. He currently focuses on semiconductor physics and silicon-based light emitting materials.